Two-Threshold Model for Scaling Laws of Noninteracting Snow Avalanches

Jerome Faillettaz
Laboratoire 3S, ENSHMG, INP de Grenoble, France

Francois Louchet
Laboratoire LTPCM, INP de Grenoble, France

Jean-Robert Grasso
LGIT, Observatoire de Grenoble, France
and USGS, Menlo-Park, California, USA
(Received 14 March 2004; published 10 November 2004)

The sizes of snow slab failure that trigger snow avalanches are power-law distributed. Such a power-law probability distribution function has also been proposed to characterize different landslide types. In order to understand this scaling for gravity-driven systems, we introduce a two-threshold 2D cellular automaton, in which failure occurs irreversibly. Taking snow slab avalanches as a model system, we find that the sizes of the largest avalanches just preceding the lattice system breakdown are power-law distributed. By tuning the maximum value of the ratio of the two failure thresholds our model reproduces the range of power-law exponents observed for land, rock, or snow avalanches. We suggest this control parameter represents the material cohesion anisotropy.

DOI: 10.1103/PhysRevLett.93.208001 PACS numbers: 45.70.Ht

Most natural avalanches, including landslides, rockfalls, turbidites, and snow avalanches exhibit scale-invariant statistics [1–4], i.e., obey power laws, $N(s) \sim s^{-b}$, where $N(s)$ is the number of events of size $\geq s$. Most often different underlying physical mechanisms in different experimental conditions may give rise to similar scaling behaviors. For the sake of simplicity, the exponents dealt with here are expressed in terms of probability distribution functions of areas in order to compare the exponents of different types of avalanches. Typical b values drawn from field data are 1.75 ± 0.3 for rockfalls and 2.8 ± 0.5 for mixed landslides [1] and references therein. Using numerical simulations [e.g. [5–14]], numerous studies have been undertaken to try to understand the origin of this scale invariance and the values of the scaling exponents. These simulations proceed as follows: a "load" variable is assigned to each site i of a grid. These variables grow through time until one of them exceeds a threshold value. The corresponding site becomes unstable, and the load is redistributed to its neighbors in either a conservative or a nonconservative way. Various relaxations are observed during a single simulation. Those models, based on Bak's sandpile model [5], reproduce qualitatively the observed scaling behavior. The exponents do not usually agree with observations except if other ingredients (e.g., dissipation or stiffness heterogeneities in [8]) or some parameter tuning are introduced [8,9].

In the case of snow avalanches, slab release results from the expansion of a "basal crack" along a weak layer parallel to the slope, followed by the opening of a "crown crack" across the slab depth as suggested by Fig. 1, (e.g., for a review see [15]). To measure the size of the snow slab failure that triggers the avalanche flow and to avoid any bias linked to the avalanche flow [e.g., as measured by acoustic emission or empirical indexes], [3,4] we use the length of the crack starting zone (Fig. 1 and 2). The exponent value of 2.2 ± 0.1 we measured for snow slab avalanches scaling is intermediate between rockfall and landslide values. Owing to their simple geometry, snow slab avalanches may be considered as a model system allowing separate treatments and sequential combinations of basal and crown failures. We designed a two-dimensional cellular automaton on this basis.

The snow slab is modeled by a 2D network of cells that have two failure modes. The first one simulates the shear failure between the snow slab and the substrate, i.e., the emergence of the basal crack. The second is the failure between two adjacent cells within the snow slab, i.e., the emergence of the crown crack (Fig. 1). The proximity to failure of a cell is defined by a single variable ζ_i propor-

FIG. 1 (color online). Snow slab failure: The slab release area is taken as L^2. The scale is given by the ski tracks that cross the bottom right of the pictures. Photograph by M. Caplain.

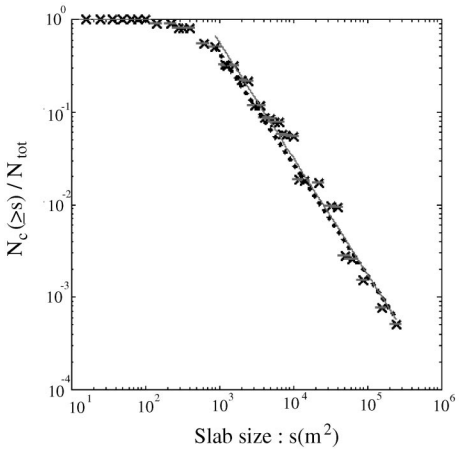

FIG. 2. Cumulative distributions of slab released areas obtained from 3935 blast triggered avalanches (Grande Plagne ski resort, France). The plateau at low sizes results from noncompleteness of reports for smaller avalanches than for larger ones. Exponent values are 1.2 ± 0.1, as estimated by the maximum likelihood method [25] for slab sizes larger than 900 m^2.

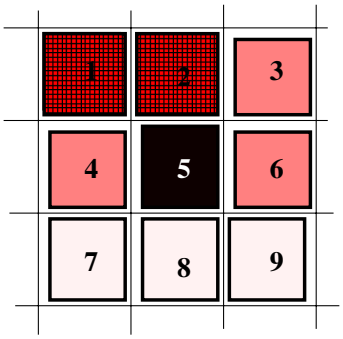

FIG. 3 (color online). Slab failure rules: (x horizontal axis, y vertical axis). Assume that the cell #5 is broken in the shear stress mode, and that load redistribution on the unbroken "upward" neighbors has occurred (shaded cells 1, 2, 3, 4, 6). Then the slab failure criterion is analyzed between cell #5 and these five upward neighbors which are located in the same x row or in higher y values. If the slab failure criterion is fulfilled for a couple of cells (e.g., stripped gray cells), the corresponding bonds between these cells break, and these cells are no longer considered as neighbors.

tional to the applied shear stress τ_a, that is initialized to 0. The lattice is initially fully intact with cells having a uniform distribution of strength thresholds. Periodic boundary conditions are taken in the horizontal direction. During each run, loading increments $\Delta\zeta$ are scattered uniformly on each cell. A cell fails in shear along the basal plane when its ζ_i value exceeds a threshold value τ_0, which brings the ζ_i value to zero. The excess ζ_i value (as well as further loading increments) is then equally redistributed onto its nonfailed first neighbors (i.e. the simulation is conservative). This implies that there is no healing process on a broken cell. A failure of the second type occurs between a cell i and one of its neighbors j when the difference $\|\zeta_i - \zeta_j\|$ exceeds a slab rupture threshold σ_0. As a consequence of load redistribution rules, which aim to simulate the slope effect, our model is polarized, i.e., the x and y directions have different behaviors (Fig. 3 and 4).

A peculiarity of our model relative to other avalanche or sandpile simulations is that, in agreement with the mechanics of snow slab failures, we introduced a second failure mode which is controlled by a finite slab strength threshold. Previous attempts using a "two state" model for sandpile dynamics either focus on flow dynamics (e.g. [16,17]) or are dissipative models (e.g.[13]). Another difference with previous studies that attempted to simulate natural slides is that there is no healing process for broken cells in our stress driven system. The system is ineluctably brought to a final instability, defined as the stage at which a macroscopic shear failure (labeled MS event in the following) occurs, and reaches the system size (Fig. 4). On our simulations we observe that each time an MS event occurs there is a remaining "C cluster" within the MS event cluster made of cells that are still unbroken in terms of slab cell interactions, i.e., in terms of the second failure mode. Following Zapperi et al. for their random fuse model [18] and by analogy to the in situ measured crack area patterns (Fig. 1), we choose the size of the cohesive C cluster to be the relevant parameter to measure the size of the simulated snow slab failure area. We checked that this measure of the last avalanche size before the breakdown of the system is not affected by the finite size of the system. In the simulation it is a proxy for the size of the largest avalanche before the final failure. In situ, it corresponds to the observed initial brittle patch of cohesive slab at the onset of the snow avalanche. After the avalanche flow, it is mapped by the crown crack length. The MS event size that is bounded by the finite size of the grid simulates the cascading effect of observed snow avalanche sliding induced by the initial snow slab failure. The system is reinitialized before each run using a uniform distribution of strength thresholds σ_0 in an interval between $\Delta\zeta$ and the shear threshold τ_0. Picking up the largest cluster (C cluster size) within the final avalanche for each run from thousands of runs leads to power-law distributions of snow slab failure sizes (Fig. 5).

The sliding dynamics of two nonplanar surfaces in contact result in strain incompatibilities and decohesions. They cannot be described solely by shear strain (controlled by a shear threshold τ_0), and the introduction of another parameter, as for instance a second failure threshold, is justified. The above model, which assigns specific thresholds to basal shear and slab cohesion failures, appears to be generic of slope failures (e.g., [14]). The power-law exponents given by our automaton can be varied by tuning a single parameter of the failure mechanism geometry, defined by $\alpha = \max[\sigma_0/\tau_0]$, i.e., the

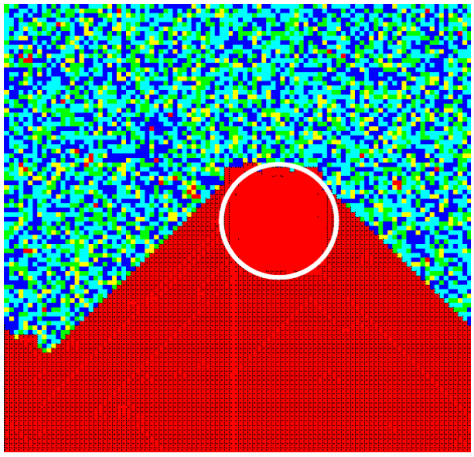

FIG. 4 (color online). Example of a simulated avalanche for 100×100 cells, (x horizontal axis, y vertical axis). Red cells (dark gray) represent shear failure between cells and substrate, and black dots intercell failures within the snow slab. During loading, some red clusters may appear, until a macroscopic cluster (labeled as MS event) suddenly forms, extends downslope (// to y axis) and reaches the limit of the grid. Cells within this red and black MS event have broken in both modes, shear failure and lateral cell failure. The C cluster (white circle) that remains within the MS event corresponds to a cluster of cells where shear failures have occurred but not slab cell failures. The 45° pattern of the MS cluster results from the load redistribution rules after a shear failure (see Fig. 3). The excess load on a cell at the lower boundary of a C cluster cannot be redistributed on its neighbors belonging to the cluster, that are already broken; they are therefore mainly redistributed on the three neighbor cells lying on the row just below.

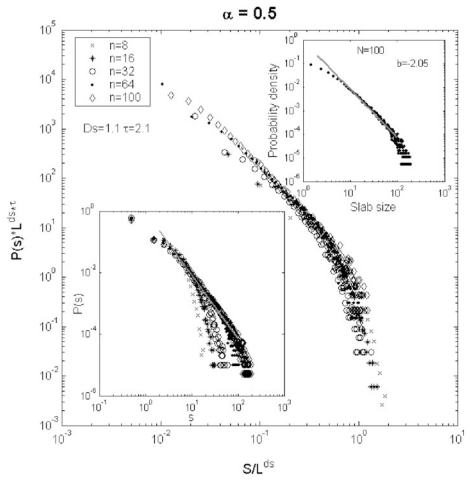

FIG. 5. Probability density of simulated avalanche size S for different system sizes, as measured by the C cluster sizes (starting zone areas); see text for details. Load increment values are $\tau_0/4$, where τ_0 is the shear threshold. For each run the ratio α of the slab cohesion and shear rupture thresholds is chosen randomly in a uniform distribution between the $\tau_0/4$ minimum value and a maximum value $\alpha = \max[\sigma_0/\tau_0]$. Taking $\alpha = 0.5$ gives a b value of 2.05 for the linear part of the plot (solid line, in the 5–100 size range, upper right inset), in agreement with the experimental results for snow avalanches (Fig. 2). The cutoff at large sizes shifts toward larger scales as the grid sizes increases, without changing the slope of the linear part of the plot (lower left inset). The finite scaling exponent used for central plot are Ds = 1.1, $\tau = 2.1$.

maximum value of the ratio of slab to shear rupture thresholds. This parameter is a possible measure of the cohesive anisotropy of the material. By tuning α, the range of observed values for the scaling exponents of the various types of gravity-driven failures can be reproduced (Fig. 6). It allows an inverse estimation of their respective cohesive anisotropies. B values of 1.75 ± 0.3 for rockfalls [1], 2.2 ± 0.1 for snow avalanches (Fig. 2), and 2.8 ± 0.5 for landslides (references in [1]) are reproduced for α values of 0.6–0.9, 0.45–0.55, 0.2–0.5, respectively. α values close to unity correspond to isotropic materials, suggesting that the more layered the material structure is, the smaller the α value (i.e. the larger b value). This is in agreement with the larger b value and the more layered structural geology reported for landslide than for rockfalls (e.g., [1]). The relatively wider range of α values for landslides may reflect a larger anisotropy scatter as compared to snow slab layer properties, e.g., [19]. For the simple geometry of snow avalanches, $\alpha < 1$ suggests a slab strength smaller than the basal shear resistance. This finding seems at first glance to contradict the general agreement that the crown crack opening during snow slab failure is a consequence of a relatively easier basal failure. This apparent contradiction is, however, removed by considering the particular type of loading experienced by the snow cover, which is essentially in shear mode parallel to the slope. Stresses acting on planes perpendicular to the slope, as for instance tensile stresses responsible for crown crack opening at the top of the slab, only arise from shear stress or shear resistance gradients. This is the reason why in our automaton the crown crack opening is controlled by the difference in ζ values between two neighboring cells. These "slab" stresses are thus usually much smaller than shear stresses acting on "basal" planes, and so our finding that the corresponding threshold may be smaller than that for basal failure is not surprising.

Increasing the α value above unity corresponds to increasing the slab failure threshold as compared to the shear failure threshold. It progressively inhibits the slab failure, which will never occur for $\alpha > 2$. Accordingly it increases the probability to observe avalanches that are just driven by the shear failure mode leading to extreme events. They correspond to a departure from the power-law behavior as evidenced as a peak in the distribution close to the cutoff value (Fig. 6). The analysis of the finite size scaling (Fig. 6) suggests that the peak may result from a finite size effect that leads the system into a supercritical state, e.g., [20].

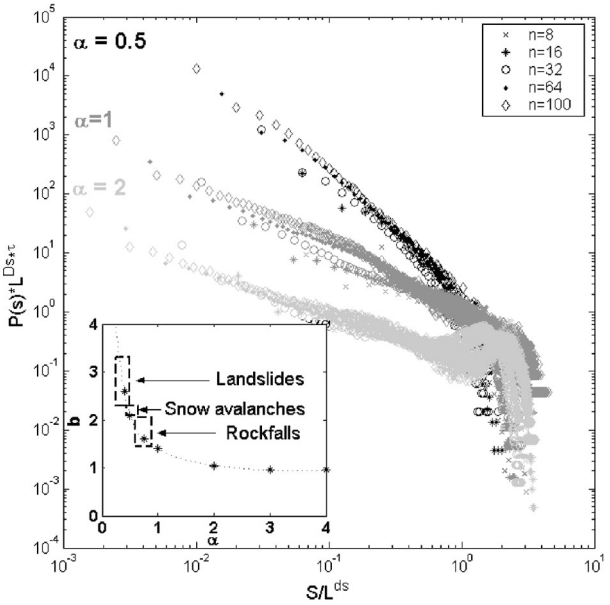

FIG. 6. Simulated avalanche size distribution as a function of α value. Same as on Fig. 5, see text for details. Insert is the evolution of the exponent of the avalanche size distribution (b value) as a function of the α values. Two regimes correspond to the activation of shear and slab failures ($\alpha < 1$, $b = f(\alpha)$) and shear failure alone, ($\alpha > 2$, $b =$ constant). The finite scaling exponent used for central plot are Ds $= 1.1$, $\tau = 2.1$; Ds $= 1.3$, $\tau = 1.4$; Ds $= 1.4$, $\tau = 1$ for α values of 0.5, 1, 2, respectively.

Our observations and model suggest that the observed power-law distributions for independent avalanches in natural gravity-driven (i.e. stress-controlled) failures may emerge from avalanches in the vicinity of a breakdown point [18] rather than from self organization: Instead of the successive relaxations recorded during a single run of stationary systems, we used as an output the size of the largest avalanche obtained for each run of a system that macroscopically fails. It corresponds to field observations in which each avalanche flow destroys the corridor or gully ability to endure a new event. As suggested by several first order transition models (e.g., [18,20,21], the scaling of the largest clusters (the C clusters) before the discontinuity may arise from the variability of either the loading values or the distance of the system from the breakdown for each of the largest avalanches. A detailed account of the results of this model as well as a complete discussion of these properties, will be reported elsewhere [22].

Introducing a two-threshold irreversible failure model, we can drive the system toward two types of behavior through variations of the ratio between these two thresholds. For $\alpha < 1$ the sizes of the last avalanche before the system breakdown are power law distributed and the exponent varies as a function of α value. It points out the possibility for our model to mimic a critical point for failure. For $\alpha > 1$, the second failure mode (i.e. slab) is progressively inhibited and α may play a role similar to the disorder in the random-field Ising model, in which there is a transition from small avalanches to a single spanning avalanche (yielding the peak in the distribution), e.g., [23] and reference therein. For all $\alpha < 1$, our rupture model suggests that standard statistical physics models for rupture (e.g., first order [18] or continuous phase transitions [24]) may possibly apply to natural avalanche phenomena as well as the sandpile simulations (e.g., [5]).

We thank A. Helmstetter, M. Wermer, and S. Zapperi for useful suggestions and discussions.

[1] C. Dussauge *et al.*, J. Geophys. Res. **108 (B6)** 2286 (2003).
[2] D. H. Rothman, J. P. Grotzinger, and P. Flemings, J. Sediment. Res., Sect. A **A64**, 59 (1994).
[3] F. Louchet *et al.*, Nat. Hazards Earth Syst. Sci. **2**, 157 (2002).
[4] K. W. Birkeland and C. C. Landry, Geophys. Res. Lett. **29**, 11 (2002).
[5] P. Bak *et al.*, Phys. Rev. A **38**, 364 (1988).
[6] P. Bak, *How Nature Works* (Springer-Verlag, New York, 1996).
[7] S. Hergarten, *Self-Organized Criticality in Earth Systems* (Springer-Verlag, Berlin, Heidelberg, 2002).
[8] L. A. Nunes Amaral and K. B. Lauritsen, Phys. Rev. E **56**, 231 (1997).
[9] Z. Olami *et al.*, Phys. Rev. Lett. **68**, 1244 (1992).
[10] D. Sornette, *Critical Phenomena in Natural Sciences* (Springer, New York, 2000).
[11] H. L. Jensen, *Self Organized Criticality* (Cambridge University Press, Cambridge, England, 1998).
[12] A. Vespignani and S. Zapperi, Phys. Rev. E **57**, 6345 (1998).
[13] S. Hergarten and H. J. Neugebauer, Phys. Rev. E **61**, 2382 (2000).
[14] A. L. Densmore *et al.*, J. Geophys. Res. **103**, 15203, (1998).
[15] Schweizer *et al.*, Rev. Geophys. **41**, 1016, (2003).
[16] J. P. Bouchaud *et al.*, Phys. Rev. Lett., **74**, 1982 (1995).
[17] S. Hergarten and H. J. Neugebauer, Geophys. Res. Lett. **25**, 801 (1998).
[18] S. Zapperi *et al.*, Phys. Rev. Lett. **78**, 1408 (1997); Phys. Rev. E **59**, 5049 (1999).
[19] S. C. Colbeck, Rev. Geophys. **29**, 81 (1991).
[20] Nunes Amaral and Lauritsen, Phys. Rev. E, **54**, 4512, (1996).
[21] P. Sethna *et al.*, Phys. Rev. Lett. **70**, 3347, (1993).
[22] J. Failletaz *et al.*, (to be published).
[23] F. J. Perez-Reche and E. Vives, Phys. Rev. B **67**, 134421 (2003).
[24] D. Sornette and J.V. Andersen, Eur. Phys. J. B **1**, 353 (1998).
[25] K. Aki, Bulletin of the Earthquake Research Institute, University of Tokyo **43**, 237 (1965).